AIChE

Kinetic Modeling Study of Carbon Nanotubes Synthesis by Fluidized Bed Chemical Vapor Deposition

R. Philippe
LCC/ENSIACET/INPT, UPR CNRS 8241, Toulouse University, 31077 Toulouse Cedex 4, France
ARKEMA LACQ Research Center, 64170 Lacq, France

P. Serp and Ph. Kalck
LCC/ENSIACET/INPT, UPR CNRS 8241, Toulouse University, 31077 Toulouse Cedex 4, France

S. Bordère, D. Plee, and P. Gaillard
ARKEMA LACQ Research Center, 64170 Lacq, France

D. Bernard
ARKEMA, 92705 Colombes Cedex, France

B. Caussat
LGC/ENSIACET/INPT, UMR CNRS 5503, 31106 Toulouse Cedex 1, France

DOI 10.1002/aic.11675
Published online December 24, 2008 in Wiley InterScience (www.interscience.wiley.com).

The kinetic and physical laws developed in the first part of the study have been implemented in a modified version of the bubbling bed Kato and Wen model to represent multiwalled carbon nanotubes (MWCNTs) synthesis by catalytic chemical vapor deposition from ethylene as carbon source and using an Fe/Al_2O_3 catalyst. The absolute deviation for MWCNT productivity between experimental results of Part 1 and simulations is of 17.3% when only considering experiments for which the bed is mainly in bubbling regime. The influence of the main operating parameters on the evolutions with time of the species molar fractions, the weight of MWCNTs formed, and the bed characteristics has been numerically studied. Such capabilities can help designing new reactors. Finally, the model has been used for scale up purposes, by increasing the reactor diameter and catalyst weight. Simulations have shown that the process productivity could reach 74 tons/year of MWCNTs in a reactor 45 cm in diameter. © 2008 American Institute of Chemical Engineers *AIChE J,* 55: 465–474, 2009
Keywords: multiwalled carbon nanotubes, catalytic CVD, fluidized bed, bubbling bed model, kinetic study, iron catalyst

Introduction

Carbon nanotubes (CNTs) synthesis represents one of the most actively explored areas in materials research of the last 10 years.[1] The kinetics of CNT growth involves complex phenom-

Correspondence concerning this article should be addressed to P. Serp at philippe.serp@ensiacet.fr. or B. Caussat at brigitte.caussat@ensiacet.fr.

ena of condensed matter self-organization, which has been mainly studied experimentally.[2] Among the hundreds of articles dedicated to CNT synthesis, only a few of them deal with the development of kinetic laws associated to numerical models able to simulate the behavior of a process of CNT production.

Zein et al.[3] studied CNT synthesis from methane using nickel supported on various materials (TiO_2, Al_2O_3, MgO, SiO_2) as catalyst in a fixed bed reactor. From gas phase chromatography (GC) measurements, they deduced kinetic laws and developed a numerical model representing a packed plug flow reactor in a kinetically controlled regime. They found a good correlation between experimental and calculated methane conversions. Endo et al.[4] developed a Computational Fluid Dynamics model to predict the production rate of CNTs from xylene in an empty tube reactor; iron was previously deposited from ferrocene on the furnace walls and a mass spectrometer was connected to the reactor exit. They deduced homogeneous and heterogeneous chemical schemes and the associated apparent kinetic laws from their experimental results. By assuming 3D, laminar, and steady state gas flow, they developed a numerical model calculating the gas velocity, temperature, and concentrations inside the empty reactor. They obtained CNT production rates in agreement with their experimental data. Gommes et al.[5] performed a kinetic study of CNT synthesis from ethylene and Fe_x-Co_y supported on alumina catalysts put in a small boat at the center of an empty quartz tube. By considering a unique first-order heterogeneous reaction, they developed 1D simple models of the gas behavior, either in purely axial convective conditions in the reactor, or in purely vertical diffusive conditions through the catalytic bed. They succeeded in predicting the ethylene reaction rate by considering simultaneously two limitations, axial convection and vertical diffusion into the fixed bed. It should be emphasized that none of these studies deals with modeling of a viable large scale production process of CNTs.

In this work, a two-phase bubbling bed model has been developed to represent the synthesis of multiwalled CNTs (MWCNTs) in a Fluidized Bed Catalytic Chemical Vapor Deposition (FB-CCVD) process. Such a process is currently employed at a semi-industrial scale for MWCNTs production.[6] The apparent kinetic equations and the physical laws of evolution of the FB features established in Part 1 of this study have thus been implemented in a modified version of the Kato and Wen model.[7,8] The main assumptions and equations of the Kato and Wen model will be first presented. The kinetic and physical laws established in Part 1 and their range of validity will be then recalled. The capabilities of the model to predict the experimental results of Part 1 and to provide information on the process behavior, in particular, to perform scale up will finally be analyzed in details.

Presentation of the Model

The Kato and Wen modified model

The main assumptions of the original Kato and Wen[7] model are as follows:

-the fluidized bed is isothermal;

-it is represented by a series of compartments whose height is equal to the mean diameter of bubbles at the corresponding level;

-bubbles are growing by coalescence as they ascend through the bed; the bubble diameter is given by the empirical relation of Kobayashi[7]:

$$D_{Bk} = D_{B0} + \lambda_k h_k, \tag{1}$$

with

$$\lambda_k = 1.4 \rho_p d_p \frac{U_k}{U_{mf}} \tag{2}$$

and

$$D_{B0} = \left(\frac{6}{\pi} \frac{U_0 - U_{mf}}{b_0} \right)^{0.4} g^{-0.2}. \tag{3}$$

The number of holes of the distributor per surface area of column b_0 is equal to 30 cm^{-2} in our case.

Each bubble is surrounded by a cloud of particles; its volume is calculated by the relation of Davidson and Harrison[9]:

$$V_C = V_B \frac{3}{\alpha_B - 1}, \tag{4}$$

with

$$\alpha_B = \frac{U_{B\infty}}{U_{mf}/\varepsilon_{mf}} \tag{5}$$

and

$$U_{B\infty} = 0.711 \sqrt{g D_B}. \tag{6}$$

-each compartment is constituted of two phases, the bubble one corresponding to the bubbles and their cloud, and the emulsion one, in which wakes are included; the volume of the bubbles for the kth compartment is given by:

$$V_{Bk} = \Delta h_k A_R \frac{U_k - U_{mf}}{U_{Bk}}, \tag{7}$$

where

$$U_{Bk} = U_k - U_{mf} + U_{B\infty k}. \tag{8}$$

The resulting volume of the emulsion for the the kth compartment is given by:

$$V_{Ek} = A_R \Delta h_k - (V_B + V_C)_k \tag{9}$$

-each phase is supposed to be perfectly mixed;

-the convective mass transfer in the emulsion phase is neglected;

-in each compartment, mass transfer occurs between the two phases and the exchange coefficient is given by the Kobayashi correlation[7]:

$$F_0 = \frac{11}{D_B} \tag{10}$$

The representation of the FB by the Kato and Wen model is illustrated in Figure 1.

Following the work of Caussat et al.,[8] we have modified the mass balance equations of the model to consider the influence of variations of gas flow rate induced by chemical reactions. Indeed, experimentally a nonnegligible increase of

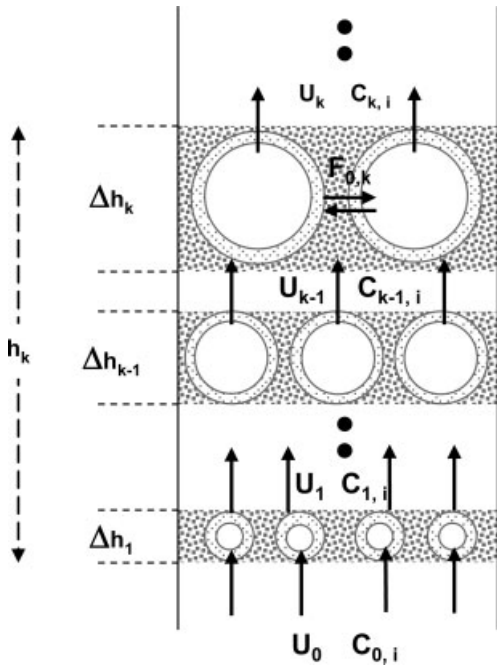

Figure 1. Representation of a fluidized bed according to Kato and Wen.[7]

the total flow rate has been observed by GC during MWCNT synthesis. The gas flow increase is due to the stoechiometry and to the relative contribution of the three reactions involved, as detailed in the next section. We have supposed that an increase of the gas flow rate creates an additional interphase transfer, leading to an increase of the bubbles volume without modification of their number. The evolution of the superficial gas velocity along the height of the bed is calculated using an overall balance equation, which is solved in each compartment of the bed. Moreover, all the parameters depending on gas velocity are recalculated in each compartment.

The modified mass balances equations are the following:

-For the bubble phase:

$$(A_R U_f C_{Bi})_{k-1} - (A_R U_f C_{Bi})_k - [F_0 V_B (C_{Bi} - C_{Ei})]_k + \left[(1-\varepsilon_{mf})\rho_p V_C r'_{Bi}\right] + (q_{EB} V_B C_{Ei})_k = 0 \quad (11)$$

-For the emulsion phase:

$$\left[(1-\varepsilon_{mf})\rho_p V_E r'_{Ei}\right]_k + [F_0 V_B (C_{Bi} - C_{Ei})]_k - (q_{EB} V_B C_{Ei})_k = 0. \quad (12)$$

The parameter q_{EB} quantifies the gaseous flux transferred from the emulsion to the bubble phase, per unit volume of bubble, due to the variation of the gas flow rate induced by the chemical reactions. It is equal to:

$$(q_{EB})_k = \frac{1}{V_{Bk}} \frac{R_{ca} T_K}{P} \rho_P \left[\left(\sum_{i=1}^{N_C} r'_{Ei} V_E (1-\varepsilon_{mf}) \right)_k - \left(\sum_{i=1}^{N_C} r'_{Bi} V_C (1-\varepsilon_{mf}) \right)_k \right]. \quad (13)$$

The resolution of an additional overall mass balance allows obtaining the evolution of the superficial gas velocity U from a compartment to another:

$$A_R (U_k - U_{k-1}) = \frac{R_{ca} T_K}{P} \rho_P \left[\left(\sum_{i=1}^{N_C} r'_{Ei} V_E (1-\varepsilon_{mf}) \right)_k - \left(\sum_{i=1}^{N_C} r'_{Bi} V_C (1-\varepsilon_{mf}) \right)_k \right]. \quad (14)$$

For each time step and for each compartment, the model solves simultaneously $2N_C$ algebraic nonlinear equations (mass balances in the bubble and emulsion phases for each of the N_C species), to access to the concentration of each gaseous species in the two phases at the exit of the compartment. The numerical method of resolution is that of Newton-Raphson. The superficial gas velocity at the exit of the compartment is then calculated by application of the overall mass balance Eq. (14) and can be recalculated if necessary by an iterative procedure. This protocol is repeated for each compartment until the sum of their height be equal to that of the expanded height calculated at the beginning of each time step with the Richardson and Zaki correlation.[10] We have verified the validity of this correlation for the catalyst/MWCNT composite powders at various contents in MWCNTs. An average superficial velocity in the bed U_{ave} is then calculated and compared with the value previously used for the estimation of the void fraction ε. An iterative procedure is applied until an agreement is found between two consecutive calculations for U_{ave} and ε.

It is worth noting that we have supposed that the slugging regime is reached when the bubble diameter equals or is higher than a limit value corresponding either to the diameter given by the relation of Grace[7,8] if this value is lower than 0.8 times the reactor diameter or to 0.8 times the reactor diameter. When the slugging regime occurred, we have arbitrarily fixed the bubble diameter to this value to perform the calculations, but the final results were clearly less precise.

Apparent kinetic equations

Let us recall that the chemical mechanism used to describe the decomposition of ethylene and the formation of MWCNTs is composed of three apparent catalytic reactions:

$$C_2H_4 \rightarrow 2C_{CNT} + 2H_2 \quad (R1)$$

$$C_2H_4 + H_2 \rightarrow C_2H_6 \quad (R2)$$

$$C_2H_4 + 2H_2 \rightarrow 2CH_4 \quad (R3)$$

Five gaseous species are then considered in the model including nitrogen.

The corresponding kinetic laws have been established from the results detailed in Part 1, by studying the influences of run duration, temperature, ethylene and hydrogen partial pressures, and iron content of the catalyst. Of course, they are only valid for the range of operating parameters we have studied. They are equal to:

$$(dX_1/dt)_{t=0} = 69.97 \times (\%_{Fe} \times m_{cata})^{0.28} \times \exp(-29,000/RT_K) \times (y_{C_2H_4})^{0.75} \quad (15)$$

Between 550 and 650°C:

$$(dX_2/dt)_{t=0} = 15.95 \times \exp(-17{,}200/RT_K) \times (y_{C_2H_4})^{1.00} \quad (16)$$

Between 651 and 750°C:

$$(dX_2/dt)_{t=0} = 6.44 \times 10^{-6} \times \exp(94{,}000/RT_K) \times (y_{C_2H_4})^{1.00} \quad (17)$$

$$(dX_3/dt)_{t=0} = 1.76 \times \exp(-17{,}000/RT_K) \times (y_{C_2H_4})^{1.37} \quad (18)$$

Let us also recall that hydrogen is necessary to these reactions but it is not considered in these kinetic laws because the productivity of each reaction is independent of the inlet hydrogen concentration as detailed in the first part of the study. So these laws are not valid when hydrogen is not injected into the reactor. It must also be recalled that these laws have been established from the initial productivities. As a consequence, this set of kinetic laws cannot represent marked temporal evolutions of productivities such as deactivation phenomena. This was not the case for our process between 650 and 750°C. On the opposite, predictions at 550°C and at a lesser extent at 600°C will be imprecise (see Part 1).

These laws have been applied at each time step, in each compartment and each phase. They have been balanced by the ratio between the solid volume present in the considered phase in the considered compartment and the total volume of solid in the bed. This balance allowed considering the dilution of the active phase occurring during deposition, because the total volume of FB increases sharply with run duration, as detailed in the next section.

Laws about the evolution of the bed physical parameters

In the first part of the study, we have determined the evolution of the main physical parameters of the FB, i.e., mean volume diameter of powders, apparent grain density, fixed bed height, and minimum fluidization velocity, with run duration.

Let us recall that the mean volume diameter of powders has been measured by laser granulometry. We observed that the void fraction of the fixed bed was independent of X_1 since the morphology of powders remained most often close to the sphere. The determination of the apparent density of powders has then been deduced from the measurement of the final fixed bed heights after MWCNT synthesis. The minimum fluidization velocity has been measured conventionally, from pressure drop measurements at decreasing gas flow rate at ambient temperature using pure nitrogen.

In a second step, we have plotted these parameters no more vs. run duration but as a function of the productivity in MWCNTs X_1, and we have verified that the fixed bed heights and the mean volume diameters of powders measured for all the other experiments of Part 1 follow the same laws of evolution vs. X_1. It appeared that the discrepancy between these two sets of values was in average of 15%. As a consequence, the model presents an intrinsic error of about 15% due to these physical laws of evolution.

The experimental points and the fitted laws are presented in details in Figure 2.

The mean volume diameter of powders increases with X_1 till a value of 1.8 g_C/g_{cata}. Beyond this productivity, catalyst grains explode and the mean diameter decreases. The final fixed bed height sharply increases with X_1, from 3 cm at $X_1 = 0$ to more than 80 cm for $X_1 = 2.7$ g_C/g_{cata}. The apparent grain density of powders consequently decreases with X_1, from 1930 kg/m^3 at $X_1 = 0$ to roughly 250 kg/m^3 at $X_1 = 2.7$ g_C/g_{cata}. These concomitant evolutions of d_p and ρ_p lead to a decrease of the minimum fluidization velocity between 0 and 0.4 g_C/g_{cata} and then to an increase of U_{mf} until values higher than its initial value, for 2.7 g_C/g_{cata}.

At the beginning of each time step, the values of d_p, U_{mf}, ρ_p, and H are recalculated from these physical laws using the current value of X_1. As determined in Part 1, the void fraction at minimum fluidization ε_{mf} has been taken equal to 0.5.

Results and Discussion

The whole operating conditions studied and the corresponding simulated results are presented in Table 1.

Comparison between experimental and calculated results

The calculated and experimental productivities of the three reactions for the experiments used to build the apparent kinetic laws (see Part 1) are compared in Figure 3. Figure 4 compares the calculated and experimental fixed bed heights and mean particles diameters for the same set of experiments. As can also be seen in Table 1, the model most often underestimates the MWCNT productivity X_1. And the whole parameters are more correctly predicted when X_1 is lower than 2 g_C/g_{cata}. This can be partly explained by the fact that high values of X_1 (>2 g_C/g_{cata}) induce high final fixed bed heights ($H > 60$ cm, i.e., $H/D > 12$), corresponding to conditions of slugging. We have already noticed that the Kato and Wen model does not correctly represent the slugging regime. Figure 4a clearly shows that the model conveniently predicts experimental fixed bed heights lower than 40 cm, mainly corresponding to bubbling conditions, whereas it underestimates the highest values corresponding to slugging conditions. So, it is likely that in this regime, the interphase gas transfer of ethylene from the bubble phase to the emulsion and then the ethylene conversion are underestimated by the model in comparison with experiments.

The absolute deviation for X_1 was of 20.8% when considering the whole results and of 17.3% when considering only the experiments for which X_1 was lower than 2 g_C/g_{cata}. This last error is close to that induced by the laws of evolution of the physical parameters and also includes the intrinsic errors of the apparent kinetic laws, in particular at 550°C. The absolute deviation was of 15.7% for X_2 and of 43.6% for X_3. This last value can be explained by the poor level of precision of the methane kinetic law as detailed in Part 1. As X_3 always remains very low in comparison with X_1 and X_2, the impact of its bad representation on the overall mechanism is low.

Finally, for the whole runs, the absolute deviations for the final fixed bed height and the mean volume diameter of grains are, respectively, 23.7% and 22.8%. Figure 4b indicates that the model most often overestimates the mean diameter of particles d_p. This result is logical since the model

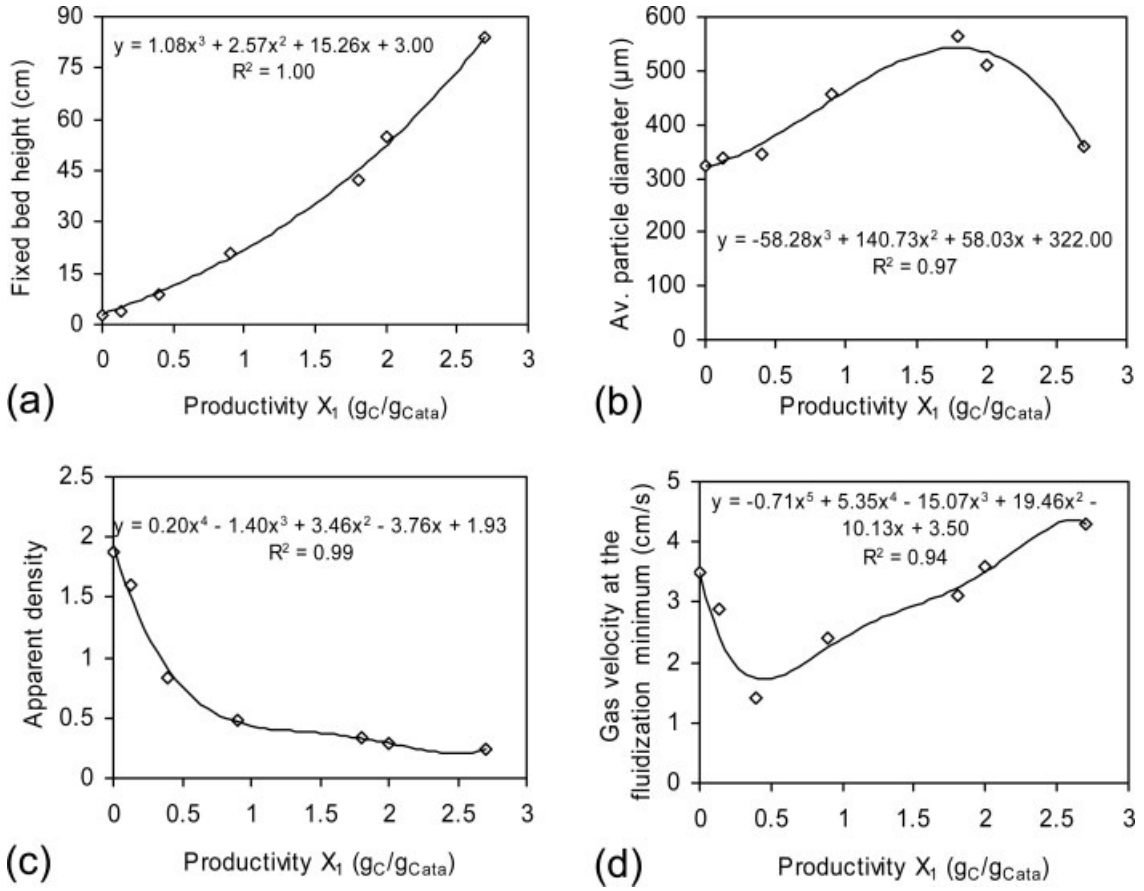

Figure 2. Physical laws of evolution of the fluidized bed and of the particles features with X_1 the MWCNTs productivity.

(a) Fixed bed height, (b) average diameter of particles, (c) apparent density, and (d) minimum fluidization gas velocity.

most often underestimates X_1 when it is higher than 2 g_C/g_{cata}, and so the mean volume diameter decreases with X_1 (see Figure 2b). As a consequence, an underestimation of X_1 results in an overestimation of d_p.

Table 1 also details the results obtained for two experiments not used to build the kinetic laws, Valid1 and Valid2. These runs have been performed in the conditions of Cin3 except the initial weight of catalytic powders. We observe

Table 1. Experimental and Simulated Results

		Experimental Results					Simulated Results				
Run	Modified Parameter	X_1 (g_C/g_{Cata})	X_2 (g_C/g_{Cata})	X_3 (g_C/g_{Cata})	H (cm)	d_p (μm)	X_1 (g_C/g_{Cata})	X_2 (g_C/g_{Cata})	X_3 (g_C/g_{Cata})	H (cm)	d_p (μm)
Cin3	–	1.8	1.04	0.079	42	564	1.56	0.92	0.063	36.5	532
Cin7	550°C	0.54	1.05	0.032	5	325	1.29	0.96	0.052	28.8	504
Cin10	600°C	1.43	1.24	0.069	25	393	1.44	0.95	0.06	33	522
Cin9	700°C	3	0.37	0.122	85	375	2	0.2	0.077	51.3	537
Cin8	750°C	2.83	0.44	0.161	78	304	2.15	0.1	0.094	57.1	522
Cin13	$y_{C_2H_4} = 0.19$	1	0.36	0.03	14	358	0.67	0.29	0.01	14.3	403
Cin11	$y_{C_2H_4} = 0.25$	1.1	0.48	0.06	16	424	0.84	0.4	0.008	17.9	433
Cin12	$y_{C_2H_4} = 0.38$	1.5	0.75	0.07	38	441	1.22	0.66	0.057	27.1	495
Cin14	$y_{C_2H_4} = 0.56$	2.5	1.01	0.1	75	459	1.72	1.05	0.09	41.7	541
Cin23	%Fe = 3.5	1.33	0.86	0.162	25	409	1.31	1.01	0.094	29.4	507
Cin24	%Fe = 5.0	1.66	0.88	0.135	35	415	1.4	0.99	0.092	31.8	517
Cin25	%Fe = 13.5	2	1.02	0.097	60	388	1.63	0.89	0.088	38.6	537
Cin1	t = 120 min	2.7	1.07	0.24	76	361	2.11	1.27	0.099	55.9	526
Cin4	t = 60 min	0.9	0.65	0.08	21	455	1.02	0.58	0.075	21.8	462
Cin5	t = 30 min	0.4	0.28	0.04	9	345	0.5	0.28	0.037	11.2	377
Cin6	t = 10 min	0.13	0.09	0.02	4	339	0.18	0.11	0.009	5.6	336
Valid1	FB weight = 200 g	0.83	0.35	0.02	70	408	0.78	0.28	0.015	67.6	424
Valid2	FB weight = 100 g	0.7	0.7	0.044	75	454	1.2	0.58	0.033	68.5	492

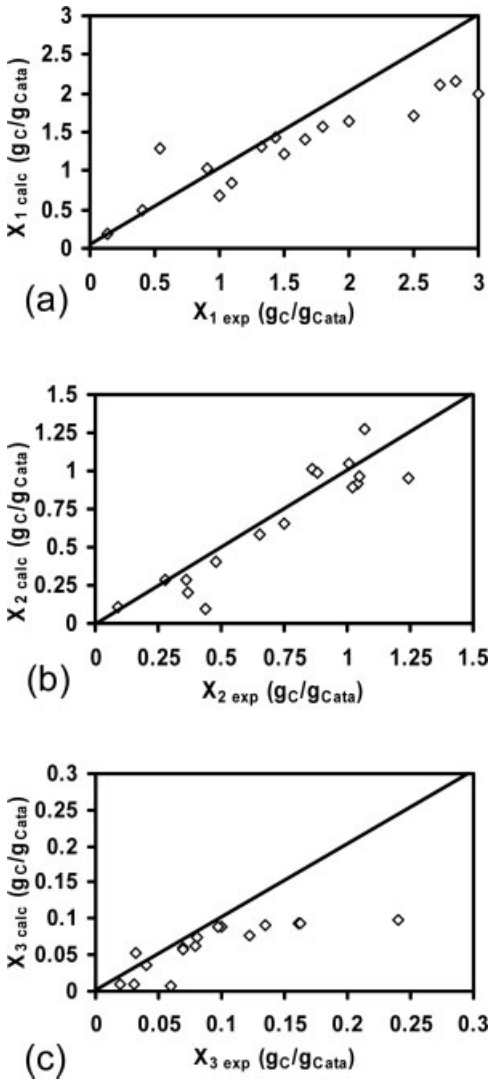

Figure 3. Comparison between experimental and simulated productivities (runs Cin1 to Cin25).

(a) X_1 MWCNTs productivity, (b) X_2 ethane productivity, and (c) X_3 methane productivity.

that the absolute deviation between experiments and simulations for X_1 is only of 5% for the two runs. The agreement is higher than for the previous set of simulations probably because the temperature for these two runs was of 650°C and the productivity in MWCNT X_1 was lower than 2 g_C/g_{cata}.

The model then provides an acceptable representation of the process as long as X_1 does not exceed 2 g_C/g_{cata} involving that the bed mainly operates in bubbling conditions.

Spatial and temporal evolutions of some process parameters

The spatial evolution of the ethylene and hydrogen molar fractions in the bubble and emulsion phases for various deposition times for run Cin3 are presented in Figure 5.

The molar fraction of C_2H_4 logically decreases along the bed whereas that of hydrogen increases. The C_2H_4 molar fraction is logically lower in the emulsion than in the bubble phase; an opposite trend is observed for hydrogen. Because of the increase of the fixed bed height with run duration and then of the dilution of the catalyst into the bed, the molar fraction of C_2H_4 at a given position into the bed increases with run duration and that of hydrogen decreases.

The appearance of the slugging regime can be easily identified in Figures 5c, d by a sudden change of the slope due to the fact that the bubble diameter and then the interphase transfer coefficient are maintained constant. This effect is much less sensible for the bubble phase than for the emulsion thanks to the existence of an intercompartment convective transfer in the bubble phase.

To illustrate the capabilities of the model, Figures 6 and 7, respectively, present the temporal evolution of the fluidization ratio, expanded bed height, and weight of MWCNTs formed during runs Cin7, Cin10, and Cin3. It appears that whatever the temperature, the fluidization ratio first increases till 20–35 min depending on the temperature and then regularly decreases. This evolution can be explained by that of U_{mf} with the productivity in MWCNTs X_1. As illustrated in Figure 2d, U_{mf} first decreases till $X_1 = 0.4$ g_C/g_{cata} and then increases. Figure 7 indicates that this value of X_1 is reached between 20 and 35 min for the runs considered. Moreover, the weight of MWCNTs and then X_1 clearly increase both

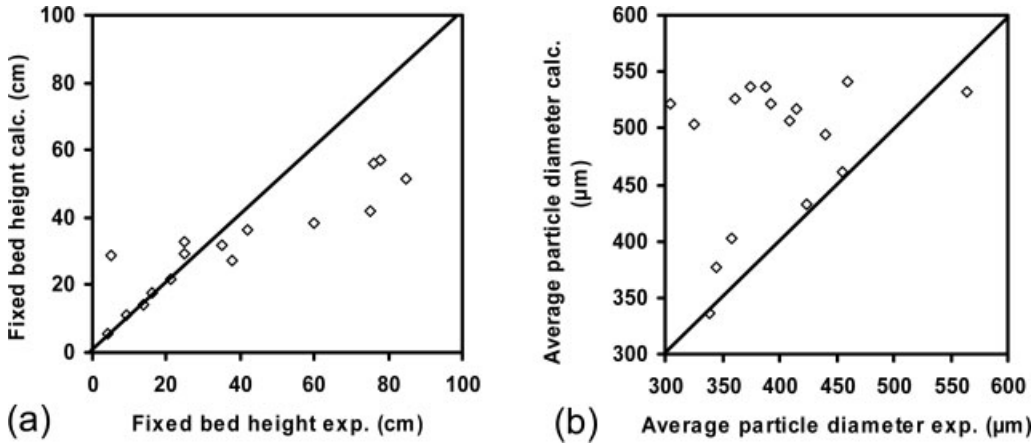

Figure 4. Comparison between experimental and simulated (a) fixed bed height and (b) average particle diameter.

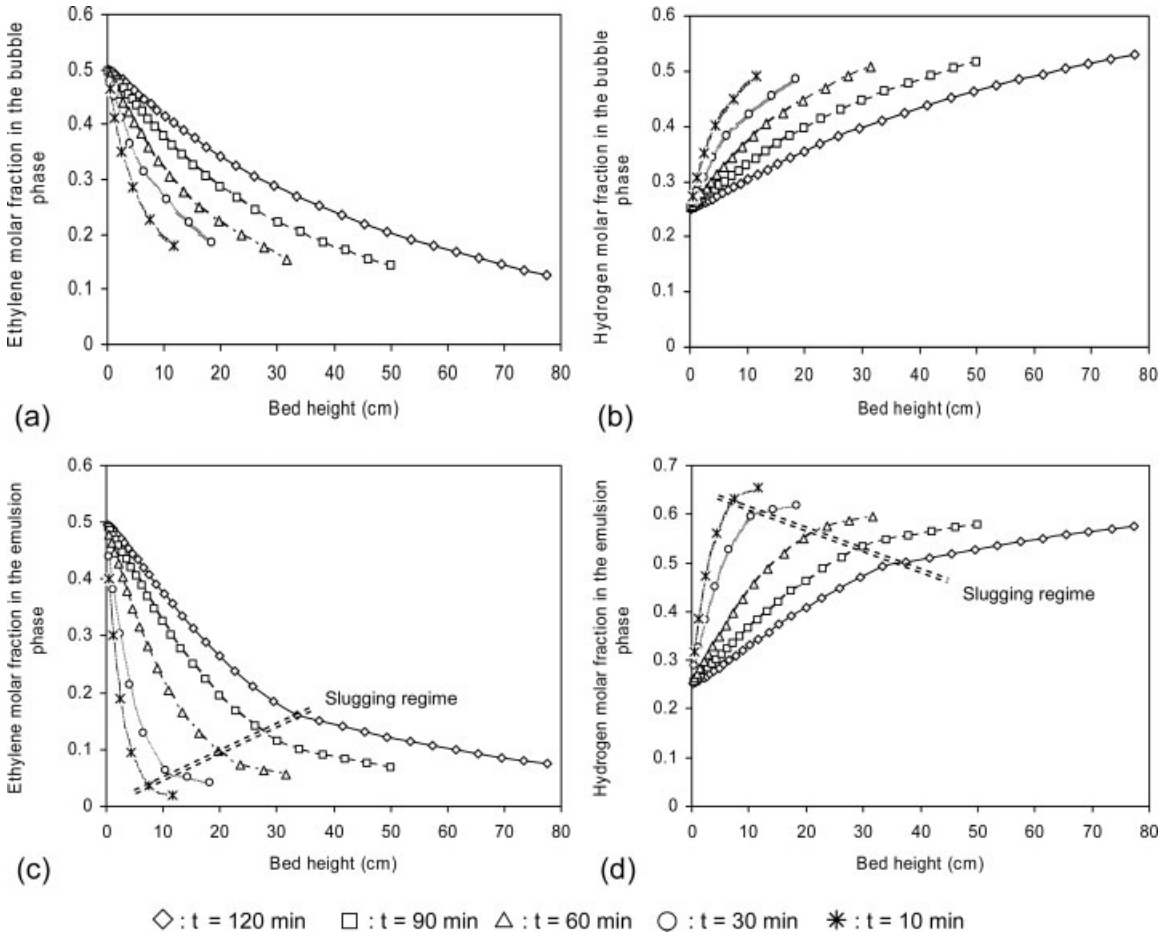

Figure 5. Axial evolution of ethylene and hydrogen molar fractions in each phase for various run durations under the conditions of run Cin3.

(a) Ethylene molar fraction in the bubble phase, (b) hydrogen molar fraction in the bubble phase, (c) ethylene molar fraction in the emulsion phase, and (d) hydrogen molar fraction in the emulsion phase.

with run duration and with temperature. It is worth noting that for the first 10 min, the weight of MWCNTs formed is quite independent of temperature, as it was experimentally observed for this catalyst (see Part 1).

As shown on Figure 6a, the fluidization ratio U_0/U_{mf} slightly increases with temperature till 20–35 min and a more marked opposite trend is observed afterward. This is due to the fact that below $X_1 = 0.4\ g_C/g_{cata}$, U_{mf} slightly

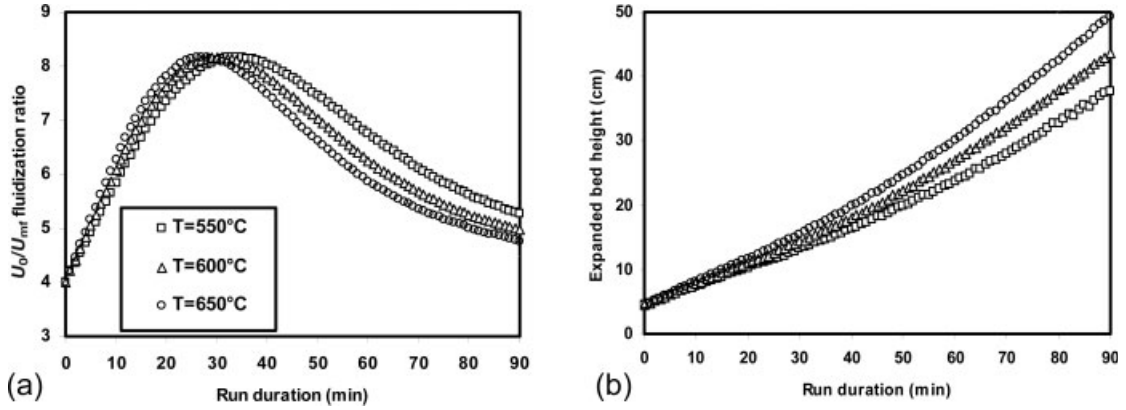

Figure 6. Simulated evolution of (a) the fluidization ratio U_0/U_{mf} and (b) the expanded bed height with run duration for various temperatures.

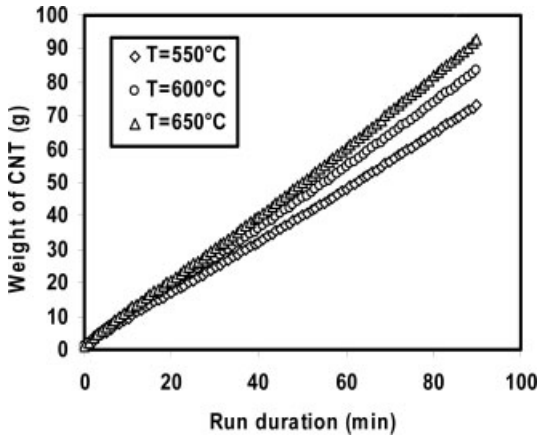

Figure 7. Simulated evolution of MWCNTs weight with run duration for various temperatures.

decreases if X_1 increases (see Figure 2d) and consequently, U_0/U_{mf} slightly increases with X_1. Beyond $X_1 = 0.4$ g_C/g_{cata}, a more marked opposite evolution exists.

It is worth noting that the temporal evolution of the fluidization ratio U_0/U_{mf} has no impact on the ethylene conversion and on the bubble diameter, since D_B (calculated using relations (1) to (3)), is controlled by the term ρ_P and not by U_0/U_{mf}. In fact, ρ_P always sharply decreases with run duration and then the bubble diameter also decreases with run duration, for a given axial position into the bed. This leads to an increase of the interphase transfer coefficient F_0, and hence to an improved gas–solid contact and logically to an enhanced ethylene conversion with run duration, for a given height into the bed. This positive effect on the conversion probably partly counter-balances the negative effect of the increase of the bed height, which favors the apparition of big bubbles and of the slugging regime, also due to the decrease of ρ_P.

The expanded bed height (Figure 6b) exponentially increases with run duration and also increases with temperature except for the first 10 min for which it is quite independent of temperature, due to the corresponding evolution of X_1.

The code could then help designing new reactors, for instance, to always maintain the FB in the heated zone and to avoid the filling of the reactive zone.

The model can also be used to explore untested operating conditions and more deeply analyze the behavior of the process. For instance, the influence of the inlet molar fraction of ethylene on various key results of the process has been studied as illustrated in Figures 8 and 9. For these simulations, the weight of catalyst (10% w/w Fe/Al_2O_3) was of 60 g, the inlet molar fraction of hydrogen was maintained at 25%, and the run duration was fixed at 60 min. Figure 8a indicates that the ethylene conversion rate decreases if the ethylene molar fraction increases, whereas an opposite trend is observed in Figure 8b for the weight of CNTs produced. These two parameters logically increase with temperature. The slope of evolution of the ethylene conversion rate with the C_2H_4 molar fraction decreases if temperature is increased. At 550°C, even if the model precision at this temperature is low, the ethylene conversion rate varies roughly between 60 and 68% whereas at 650°C, it varies only between 72 and 76%. It is then more interesting to work at 650°C and at high ethylene molar fraction to reach the highest productivities in MWCNTs while maintaining quite high ethylene conversion.

Figures 9a, b show that the final expanded bed heights and grain diameters increase both with the ethylene inlet molar fraction and temperature. These evolutions are logical because they follow that of the final MWCNT weight (Figure 8b). It appears that for the conditions tested, the expanded bed height after 1 h of run has increased by a factor 3–9 depending on the inlet ethylene molar fraction and temperature, whereas the mean grain diameter has only increased by a factor of 1.1–1.5. Such evolutions are important to know a

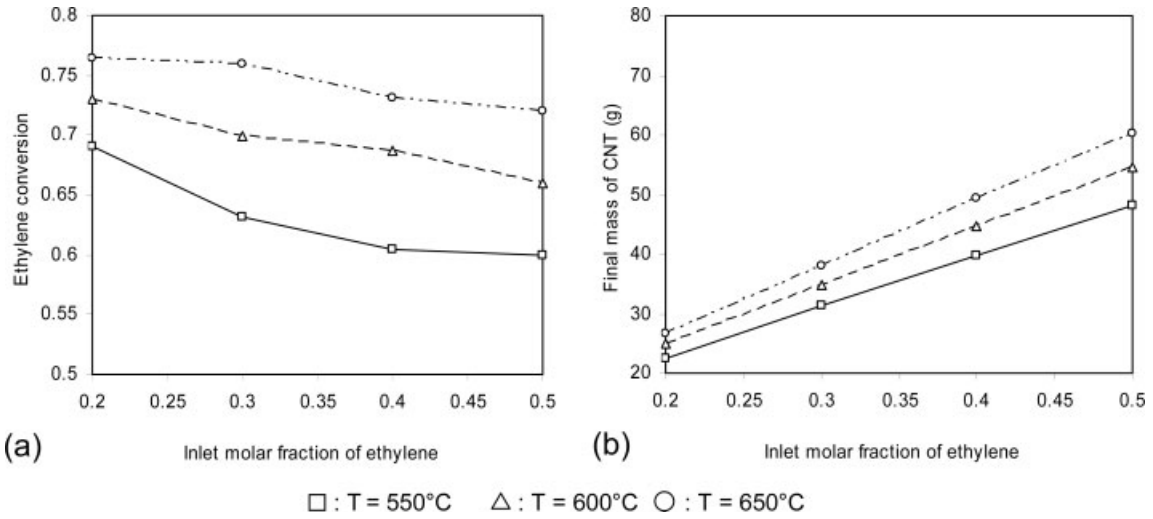

Figure 8. Influence of the inlet molar fraction of ethylene on (a) the ethylene conversion rate and (b) the final mass of MWCNTs for various temperatures.

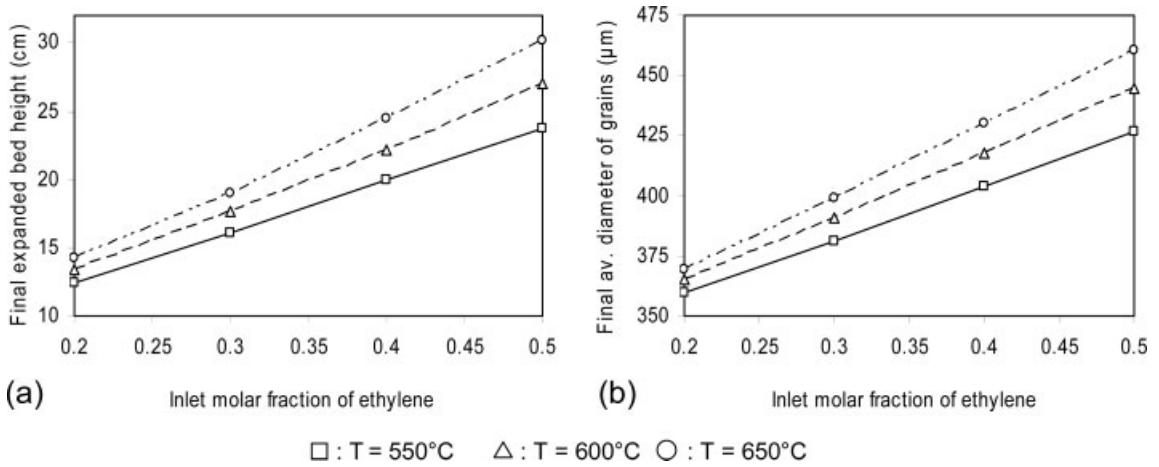

Figure 9. Influence of the inlet molar fraction of ethylene on (a) the final expanded bed height and (b) the mean grain diameter for various temperatures.

priori for instance to perform scale up and to find optimal residence times of powders if the scaled up processes work in continuous mode.

Simulation of various process scale up

One of the main interests of the model also lies in the possibility to simulate FB-CCVD reactors of higher dimensions to prepare possible scale up of the process. To illustrate this ability, three simulations have been performed under the conditions of the nominal run Cin3 for reactor inlet diameters, respectively, equal to 15, 25, and 45 cm. The weight of catalyst has been adjusted so that the initial fixed bed height is identical to that of the nominal run, i.e., 3 cm.

These simulations correspond to runs Extra1, Extra2, and Extra3 of Table 2. It is worth noting that the slugging regime never occurred for these simulations since the ratio between the final fixed bed height and the reactor diameter H/D never exceeded 3.2. This strengthens the validity of these predictions.

It can be observed that the productivity X_1 and the selectivity in MWCNTs regarding the formation of ethane and methane increase with the reactor diameter. This improvement of the process performances is probably due to a better interphase contact. Indeed, the ratio between the bubble diameter and the reactor diameter is clearly lower when increasing the reactor diameter. As a consequence, for the conditions tested, the slugging regime never appears and the bubbling regime exists all along the run durations, even for MWCNT productivities X_1 higher than 2 g_C/g_{cata}.

The weight of MWCNTs reaches 13.2 kg in 90 min for the reactor of 45 cm in diameter. This corresponds to 211 kg/day or to about 74 tons/year of MWCNTs for a semi-industrial pilot reactor working 24 h/day and 350 days/year in semibatch conditions. This capacity of production fully demonstrates the interest of the process to produce in mass these nanomaterials.

Conclusions

A model of fluidized bed has been developed to represent MWCNTs synthesis by Catalytic Chemical Vapor Deposition from ethylene as carbon source and using an Fe/Al_2O_3 catalyst. The kinetic and physical laws developed in Part 1 have thus been implemented in a modified version of the Kato and Wen model. To the best of our knowledge, this is the first time that a two-phase bubbling bed model is used to simulate a viable process of large scale MWCNTs production. Its domain of validity is of course restricted to the operating range used to develop the associated kinetic and physical laws. Its accuracy is also limited by the fact that the kinetic laws are not intrinsic and do not account for any deactivation phenomenon.

The model has first been used to predict the experimental data of Part 1. The absolute deviation for MWCNT productivity between these experimental results and the simulations was of 20.8% for the whole data and of 17.3% when considering only experiments for which the bed was mainly in bubbling regime. A perspective of the work could then be to

Table 2. Simulation of Various Process Scale Up

Simulation	Reactor Diameter (cm)	Catalyst Weight (kg)	$(H/D)_0$	CNT Weight (kg)	X_1 (g_C/g_{Cata})	X_2 (g_C/g_{Cata})	X_3 (g_C/g_{Cata})	d_p (μm)	H (cm)	H/H_0	H/D
Cin3	5	0.06	0.6	0.094	1.56	0.92	0.063	532	36.5	12.2	7.3
Extra1	15	0.49	0.2	1.125	2.30	0.73	0.045	496	48.8	16.3	3.2
Extra2	25	1.36	0.12	3.588	2.64	0.63	0.038	297	64.7	21.6	2.6
Extra3	45	4.4	0.067	13.206	3.00	0.52	0.030	285	120	40	2.7

implement these kinetic and physical laws in a slugging bed model[11] or in an Eulerian multifluid model-like MFIX[12] to better represent the hydrodynamics of the fluidized bed in particular in slugging regime and the associated interphase mass transfers.

The code has also allowed to calculate the influence of the main operating parameters on the evolutions of the species molar fractions and on the bed characteristics vs. run duration. This numerical tool can then help to better control the evolution with time of the process behavior, for instance, in terms of fluidization regime, mean diameter of grains, or expanded bed height.

In a last part, the influence of the bed features as the reactor diameter and weight of catalyst has also been studied proving the interest of such model for scale up. Simulations have shown that the productivity in MWCNTs could reach 8 kg/h in a 45-cm diameter reactor operating in semibatch conditions. This corresponds to around 74 tons/year of MWCNTs selectively produced. An increase of reactor diameter provides better interphase contacts due to lower bubble diameters, relatively to reactor diameter, and then enhances the process productivity in MWCNTs and its selectivity regarding ethane and methane. The interest of the process to massively produce MWCNTs is then fully demonstrated.

Notation

A_R = column section area (m^2)
b_0 = number of holes of the distributor per surface area of column (m^{-2})
C_B = concentration of the bubble phase (mol/cm^3)
C_E = concentration of the emulsion phase (mol/cm^3)
d_p = volume median diameter of particles (μm)
D = reactor diameter (cm)
D_B = bubble diameter (cm)
D_{B0} = initial bubble diameter (cm)
F_0 = interphase mass transfer coefficient (s^{-1})
g = gravity (m/s^2)
h_k = height above the distributor of the kth compartment (cm)
H_0 = initial fixed bed height (cm)
H = final fixed bed height (cm)
m_{cata} = weight of catalyst into the bed (g)
N_C = number of gaseous species in the system
P = total pressure (Torr)
q_{EB} = interphase transfer due to the increase of the total number of moles (s^{-1})
Q_i = inlet flow rate of the gaseous species i (l/min STP or slm)
r'_{Bi} = kinetic rate for species i in the bubble phase (mol/(g s))
r'_{Ei} = kinetic rate for species i in the emulsion phase (mol/(g s))
R = constant of perfect gases (8.32 J/(mol K))
R_{ca} = constant of perfect gases (62361 (cm^3 Torr/(mol K)))
R_{CNT} = ethylene conversion rate (%)
S = selectivity of the process (from *: low selectivity, to ****: excellent selectivity)
T = bed temperature (°C)
T_K = bed temperature (K)
U = superficial velocity of gas (cm/s)
U_0 = inlet superficial velocity of gas (cm/s)
U_B = velocity of bubbles (cm/s)
$U_{B\infty}$ = velocity of an isolated bubble (cm/s)
U_{ave} = average superficial gas velocity along the bed height (cm/s)
U_{mf} = minimum velocity of fluidization (cm/s)
V_B = volume of bubbles (cm^3)
V_C = volume of cloud (cm^3)
V_E = volume of emulsion (cm^3)
X_i = productivity for reaction (R_i) (g_C/g_{cata})
y_i = molar fraction of species i

Greek letters

α_B = ratio of gas velocities defined by relation (5)
Δh_k = height of the compartment k (cm)
ε_{mf} = void fraction of the bed at minimum fluidization
ρ_p = apparent grain density (g/cm^3)
k = subscript relative to the kth compartment

Literature Cited

1. See CH, Harris AT. CaCo3 supported Co-Fe catalysts for carbon nanotube synthesis in fluidized bed reactors. *AIChE J*. 2008;54:657–663.
2. Louchev OA. Transport-kinetical phenomena in nanotube growth. *J Cryst Growth*. 2002;237–239:65–69.
3. Zein SHS, Mohamed AR, Sai PST. Kinetic studies on catalytic decomposition of methane to hydrogen and carbon over Ni/TiO_2 catalyst. *Ind Eng Chem Res*. 2004;43:4864–4870.
4. Endo H, Kuwana K, Saito K, Qian D, Andrews R, Grulke EA. CFD prediction of carbon nanotube production rate in a CVD reactor. *Chem Phys Lett*. 2004;387:307–311.
5. Gommes C, Blacher S, Bossuot C, Marchot P, Nagy JB, Pirard JP. Influence of the operating conditions on the production rate of multi-walled carbon nanotubes in a CVD reactor. *Carbon*. 2004;42:1473–1482.
6. Philippe R, Morançais A, Corrias M, Caussat B, Kihn Y, Kalck P, Plee D, Gaillard P, Bernard D, Serp P. Catalytic production of carbon nanotubes by fluidized bed chemical vapor deposition. *Chem Vap Deposition*. 2007;13:447–457.
7. Kato K, Wen CY. Bubble assemblage model for fluidized bed catalytic reactor. *Chem Eng Sci*. 1969;24:1351–1369.
8. Caussat B, Hemati M, Couderc JP. Silicon deposition from silane or disilane in a fluidized bed, Part 2: theoretical analysis and modelling. *Chem Eng Sci*. 1995;50:3615–3624.
9. Davidson JF, Harrison D. *Fluidized particles*. New York: Cambridge University Press, 1963.
10. Richardson JF, Zaki WN. Sedimentation and fluidization, Part 1. *Trans Inst Chem Eng*. 1954;32:35–42.
11. Constantineau JP, Grace JR, Lim CJ, Richards GG. Generalized bubbling-slugging fluidized bed reactor model. *Chem Eng Sci*. 2007;62:70–81.
12. Cadoret L, Reuge N, Pannala S, Syamlal M, Coufort C, Caussat B. Silicon CVD on powders in fluidized bed: experimental and multifluid Eulerian modelling study. *Surf Coat Technol*. 2007;201:8919–8923.

Manuscript received Feb. 22, 2008, and revision received July 15, 2008.